International Journal of Non-Linear Mechanics 138 (2022) 103837

Contents lists available at ScienceDirect

International Journal of Non-Linear Mechanics

journal homepage: www.elsevier.com/locate/nlm

Investigation on buckling and mode jumping of composite plates under thermomechanical loads

Javier Gutiérrez Álvarez, Chiara Bisagni *

Delft University of Technology, Faculty of Aerospace Engineering, Kluyverweg 1, 2629 HS Delft, The Netherlands

ARTICLE INFO

Keywords:
Buckling
Composite plates
Thermomechanical
Finite element analysis
Mechanical testing
Thermal testing

ABSTRACT

This paper presents an experimental and numerical study of composite plates, analyzing the interaction between mechanical and thermal loads related to buckling and the occurrence of mode jumping. A novel experimental setup for thermomechanical testing was developed. The setup is conceived around a frame with a low coefficient of thermal expansion, so that the plate can experience buckling and mode jumping when heated; and when compressed, interactions between the two loading states can be studied. Experimental results of plates loaded under diverse load cases are delivered in the form of load vs out-of-plane deflection graphs, deflection plots and buckling charts, where all buckling and mode jumping bifurcation points are registered. The influence of combined loading over mode jumping phenomena was successfully captured. Numerical predictions are able to estimate general tendencies in the occurrences of both buckling and mode jumping and in the mutual influence of thermal and mechanical loads.

1. Introduction

Aerospace structures are often required to work under conditions that involve combinations of mechanical and thermal loads, while accomplishing conflicting requirements such as robustness and being lightweight. Such requisites often yield thin-walled structural designs which are highly mass efficient but also vulnerable to buckling. Buckling has been traditionally considered as a liability or as a "no-go" area, even though, under specific circumstances, buckling can be used to enhance the aircraft structural performance [1]. In these cases, post-buckling regime states are considered as an extension of the original operative range of a given structure. While mechanically buckled structures have been successfully exploited in the past to improve structural performance, thermal buckling has traditionally been avoided [2]. However, thermally post-buckled states have been also successfully applied through the use of beaded panels or corrugated structures [3,4], seeking aims such as increasing buckling stiffness or relaxation for thermal stresses. Structural elements as plates have potential for such applications, because of their stable behavior in post-buckling regime. Carbon fiber reinforced plastics (CFRP) materials can greatly contribute to this aim due to the high structural performance they offer and their material behavior that allows for large elastic deformations. They also offer high design flexibility thanks to the possibility to optimize their stacking orientation. Good knowledge of thermomechanically buckled states can help structural designers to identify potential advantage opportunities, make better choices and eventually contribute to better future designs.

On the other hand, new research trends are putting traditional conceptions about buckling under revision, as they are willing to observe buckling as a structural state with potentially advantageous features [5–7]. Gutiérrez Álvarez and Bisagni [8] performed experiments in heated, rectangular, symmetric and balanced angle-ply composite plates. The plates were able to display shape changes in the form of mode jumps when assembled in a stiff constraining fitting with low coefficient of thermal expansion (CTE). Cases in which plate size remains constant are, however, an idealization: a plate attached to an airframe is subjected to stretching and compression due to service loads. Plate size variation has a direct impact over the buckling temperature [9], while the impact over the mode jumping temperature is unknown.

Taking a look over previous work, the interest in thermal buckling emerged with the beginning of supersonic flight [10,11]. Throughout the decades, the focus evolved, ranging from innovative structural configurations and geometries to the introduction of new generation aerospace materials. Thermal buckling experiments can be roughly divided in two types. The first type refers to tests in which the specimens buckle by stresses arisen due to constrained size variations. During the test, the specimen, typically a flat plate, is installed within a restraining fixture, sometimes water-cooled, and subjected to a typically uniform temperature increase. Examples are the tests on metallic plates performed by Murphy and Ferreira [12] or the tests on metal foam core sandwich panels done by Rakow and Waas [13]. In composite materials, Amabili et al. [14] tested the buckling of cooled composite plates; Wu and Gurdal tested heated steered fiber panels, and more recently Xu et al. [15] tested the buckling C/SiC woven composite plates.

* Corresponding author.
E-mail address: c.bisagni@tudelft.nl (C. Bisagni).

https://doi.org/10.1016/j.ijnonlinmec.2021.103837
Received 5 August 2021; Received in revised form 5 October 2021; Accepted 18 October 2021
Available online 29 October 2021

A subtype of test is the case where free, unrestrained plates buckle merely due to thermal gradients [16]. Ehrhardt and Virgin [17] found the presence of alternative equilibrium states in rectangular, metallic, thermally buckled plates, Bhagat and Yeyaraj [18] studied the effect of non-uniform temperature distributions on the thermal buckling of shallow curved metallic panels, and Gutiérrez Álvarez and Bisagni [8] achieved buckling and mode jumping in carbon composite plates. The second type of thermal buckling tests available in literature consists on specimens being placed in a compression device and subsequently being subjected to combinations of compression and heat. Substantial experimental efforts were made during the early test campaigns of Ross et al. [19], Anderson and Card [20], Mayers and Jaworski [21], Bushnell [22], Frum and Baruch [23] and Ari-Gur and Baruch [24]. All these experiments were performed considering metallic cylinders, heated either uniformly or along two opposite cylinder generators. Percy and Fields [25], and Thompson and Richards [26] tested identical hat stiffened panels made in titanium and titanium matrix composite under the simultaneous effect of compression and heat. Still, the most sophisticated experimental setups available are based in multi-actuator concepts, such as the one developed by Fields [27] who developed a test setup for combined thermomechanical loading using an 8-engine system capable of exerting compression, tension and/or shear with heating loads over a flat stiffened panel, or the Nasa Langley Combined Loads Testing System [28]. The amount of available literature on experiments on thermomechanical buckling is, however, not extensive, being this scarcity even more pronounced for CFRP structures. On shallow shells, Breivik and Hyer [29] tested shallow shells made in composite material, with different layup under either heating or compression. Even if considerable efforts have been made in the field of buckling and post-buckling of composite structures [30–33], understanding instabilities triggered by thermomechanical loads [34], and also in understanding the mode changes in thin-walled structures [35,36], no experimental attempts can be easily found on understanding mode changes in thermally and mechanically loaded composite plates.

The goal of this research is to perform an exploratory investigation to evaluate the effects of combined thermal and mechanical loads over buckling and mode jumping in CFRP plates, with the purpose of understanding the mutual interaction of these loads in post-buckling regime, as well as possible implications for real applications. During this investigation both numerical and experimental techniques were used, even if the principal focus is the development and implementation of a novel experimental methodology and the presentation of a set of preliminary results. The proposed setup is based on the previously used concept of utilizing a low CTE invar frame to restrain thermal expansion [8], which is upgraded by incorporating the novel concept of applying compression to the frame using a compression machine. The proposed setup is therefore capable to simultaneously apply compression and heat. Tested plates have a laminate stacking that can both buckle and show mode jumps when heated, compressed, or under combination of these two loading conditions.

In Section 2, the main concepts related to the analyzed phenomena are introduced; in Section 3, numerical predictions performed using the Finite Element software Abaqus are presented and discussed. Section 4 contains a description of the experimental setup. In Section 5, a set of preliminary experimental results are presented: in particular, results for each type of performed test are reported in the form of load vs. displacement graphs and out-of-plane deflection shapes. A final experimental buckling chart for combined loading is also reported with the results of all performed tests. A discussion about the obtained results and the deviations from the numerical predictions is presented, and potential sources of error are discussed.

2. Buckling and mode jumping on heated and mechanically loaded composite plates

A mode jump can be described as a change in the buckling shape of a panel as a consequence of variations in the load. This phenomenon often occurs in an abrupt manner and can be thus considered a dynamic event. In order to better explain this phenomenon, it is convenient to use an idealized plate such as the one represented in Fig. 1.

A rectangular flat plate of width a, height b and thickness t, made in composite laminate material, with a symmetric and balanced stacking orientation is considered. A XYZ coordinate system is placed in the lower left corner of the plate, coinciding the XY plane with the mid plane of the plate. Displacements along the axis are characterized as U, V, W. Rotations around the four plate edges are constrained, and also the out-of-plane displacements of the edges are constrained. The plate is not allowed to experience change in size along X direction i.e. $\Delta_x = 0$, while external mechanical load along Y can be introduced in the form of a prescribed vertical displacement Δ_y. The plate can also be loaded by introducing uniform temperature increments ΔT. Positive values of ΔT correspond to temperatures over the in-plane stress free temperature, while negative values of Δ_y correspond to a shortening of the plate, i.e. compression. Plate edges remain straight during the whole loading process. The plate can therefore be subjected to combinations of loading conditions ΔT and Δ_y, from now on referred as load cases.

Different load cases are analyzed. A "*pure heating*" load case assumes that a ΔT is applied while Δ_y remains fixed at 0 mm; in a "*pure compression*" load case Δ_y is applied while ΔT is zero. A combined "*compression + heating*" load case consists of two load phases: during the first one a compressive Δ_y is introduced, and in the second loading phase a ΔT is applied on top of the initial Δ_y. The order of load application is relevant. During this investigation, two combined load cases are considered, "*compression + heating*" and "*heating + compression*".

When the plate is subjected to an homogeneous, monotonically increasing ΔT in a "*pure heating*" load case, stresses arise as a consequence of restrained thermal expansion. The typical path of the deflection at the plate center can be followed in Fig. 2. With temperature increasing, the plate remains flat till a bifurcation point, known as buckling temperature ΔT_{b1}, is reached. Once buckling temperature is surpassed, the plate starts to deform out of plane following the path reported as a bold black line, usually in a shape with a sinusoidal half-wave in the X direction and a sinusoidal half wave in the Y direction, denoted as a $(1,1)$ shape. If the value of ΔT keeps growing, plates with certain layups may encounter bifurcations and change into different stable buckling shapes, typically into a $(1,2)$ or $(2,1)$ shape. This occurrence is commonly known as a mode jump or mode change and it is reported in the figure as temperature ΔT_{b2}. This is a well-known occurrence, which has been extensively documented for mechanically loaded metallic and composite panels [37–41]. The magnitude of ΔT_{b2} and also the mode shape obtained after the jump are heavily dependent on the dimensions, stacking orientation and boundary conditions of the plate.

If the plate is instead subjected to a "*compression + heat*" load case, a compressive Δ_y is first applied, and then a ΔT is gradually introduced. Buckling temperature ΔT_{b1} is expected to decrease with the magnitude of initial compression Δ_y [9]; this mechanical pre-load is expected to have also an impact over the mode jumping temperature ΔT_{b2}, typically a decrease, as shown in Fig. 2. However, the relation between the applied Δ_y and the obtained reduction of ΔT_{b2} is a priori unknown, and such phenomenon happens in the nonlinear regime where linear load superposition is not expected to hold.

When the plate is loaded under a "*pure compression*" load case, the plate deflections may describe a trajectory analogue to the "*pure heating*" case: buckling is reached at displacement $\Delta_{y,b1}$, and a mode jump may occur at $\Delta_{y,b2}$. Contrary to the "*pure heating*" load case, the orientation of the mode jump is strongly preconditioned by the direction of the compressive load: an initial (1,1) buckling shape can be followed by a (1,2) buckling shape, as the main compressive load comes from that direction. Preloads in the form of initial ΔT, in the "*heat + compression*" load case, are expected to reduce $\Delta_{y,b1}$ and $\Delta_{y,b2}$.

These deflection paths correspond to the behavior of a perfectly flat plate. In reality, plate imperfections are unavoidable and have a

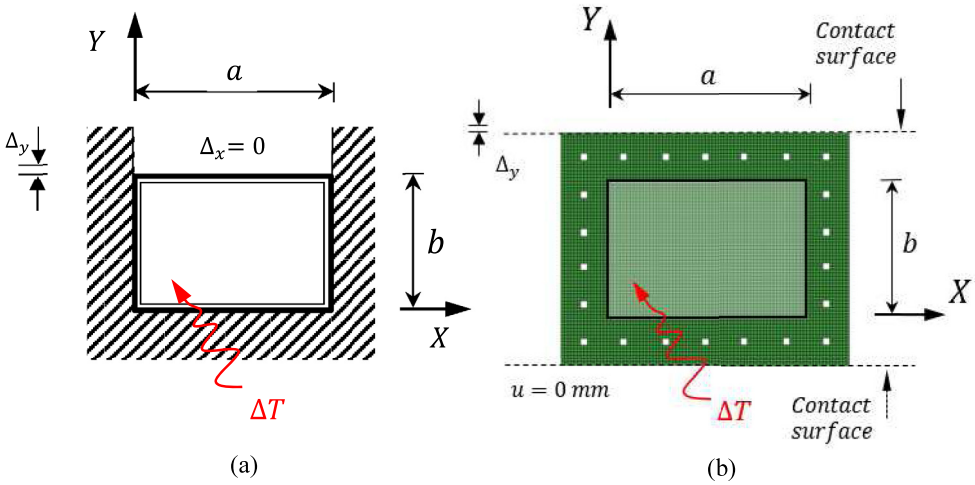

Fig. 1. Plate under thermal and mechanical loads: (a) Plate boundary conditions; (b) FE model.

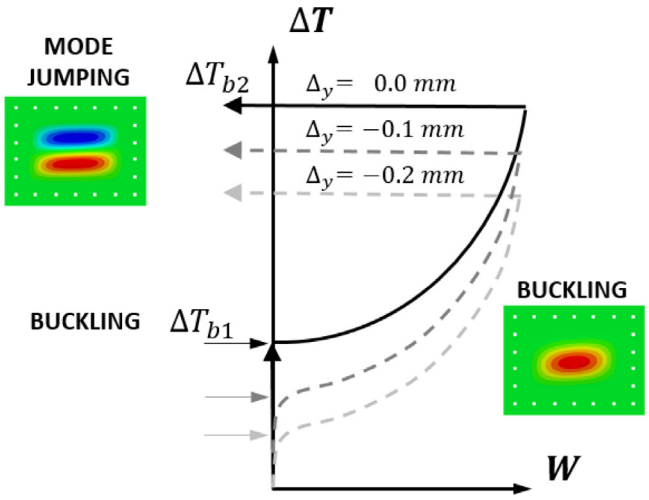

Fig. 2. Mode jumping under thermal and mechanical loads.

substantial effect over the overall plate behavior [8]. Real boundary conditions are also to be taken into consideration: in particular, the material of the boundary conditions may be sensitive to temperature changes, and thus experience size variations when subjected to a ΔT. This can have an impact on both buckling and mode jumping temperatures of the plate.

3. Preliminary analysis: mode jumping in plates subjected to thermal and mechanical loads

Two different types of numerical procedures were conducted as preliminary analysis of the considered structure: a linear eigenvalue analysis and a dynamic explicit analysis.

Both types of simulation were performed using the same finite element (FE) model performed in Abaqus, shown in Fig. 1(b). The model is a simplification of the proposed experimental configuration: the compression machine in the real test setup was not represented in the model; instead, only the plate and the frame were modeled. The FE model represents a plate of size 440 mm × 340 mm, made in composite material $AS4/8552$, fixed on a surrounding structural frame made in Invar 36. The frame and the plate have the same width and height of 440 mm × 340 mm; when they are assembled together, a smaller area of the plate with dimensions 300 mm × 200 mm remains accessible; this area corresponds to the region with width a and height b reported in Fig. 1. The material properties are reported in Table 1. The plate has a stacking orientation $[35/-35/10/-10]_s$. This stacking was successfully used in previous experimental campaigns to reproduce thermal buckling and mode jumping in composite plates [8]. The FE model consists of standard quadrilateral shell elements $S4R$ with a size of 5 mm. The elements of the plate and the frame have nodes at identical positions, and thus were tied together, therefore seamlessly connected, which means no slipping due to gripping loss nor effect of friction between frame and specimen were considered. Vertical displacements V in the lower contact surface of the frame were constrained; out-of-plane deflections W were constrained at both lateral edges. Load introduction was performed by enforcing Δ_y as vertical displacement V over the upper contact surface of the frame, and/or by enforcing ΔT in all nodes in the model.

For a given FE simulation, the corresponding load case is implemented by introducing the different loading phases as steps in the analysis. In a linear eigenvalue analysis, the first load phase is introduced as a general static analysis, and the second load phase is introduced in the form of an eigenvalue analysis over the preloaded structure. In a dynamic explicit analysis, loading phases are implemented as load steps where the load is introduced as loading ramps, with loading speeds of −0.05 mm/s and 3° C/s for compression and heating phases, respectively. These loading rates are significantly higher than the experimental counterparts, and were verified to decrease the analysis time without affecting the final result. An imperfection with the shape of the first eigenvalue analysis, with amplitude of 0.5% of plate thickness, was assumed. Such imperfection amplitude is comparatively small, and thus grants a behavior close to the perfectly flat plate.

The results of the eigenvalue analysis and the dynamic explicit analysis are reported in Fig. 3, where ΔT is plotted versus Δ_y. White and magenta colored markers indicate buckling and mode change bifurcations, respectively. Marker shape provides information about the loading condition operating at the moment of bifurcation: circular and triangular marker shapes denote compression and heat loading, respectively.

Considering a *"pure compression"* load case, the loading path starts at the origin and follows the horizontal axis till a bifurcation point is found at $\Delta_{y,b1} = -0.120$ mm; this is reported in the graph with a white, circular marker at position $(-0.120\ \text{mm}, 0°\text{C})$. Under *"pure heating"* conditions, the loading path overlaps with the vertical axis and buckling is reached at $\Delta T_{b1} = 43.81°\text{C}$; reported over the vertical axis as a white triangular marker. The other white markers reported in the graph represent buckling results for combined load cases: for instance, when an initial load of $\Delta_y = -0.02$ mm is applied and temperature is increased, buckling is found for $\Delta T_{b1} = 36.68°\text{C}$; the analysis is registered

Table 1
Material properties.

	E_{11} [GPa]	E_{22} [GPa]	G_{12} [MPa]	ν_{12}	α_1 [μm/m°C]	α_2 [μm/m°C]	t_{ply} [mm]	ρ [kg/m^3]
AS4/8552	135	9.68	5.6	0.30	0.28	28	0.181	1.58
Invar 36	140			0.33	1.5			8.05

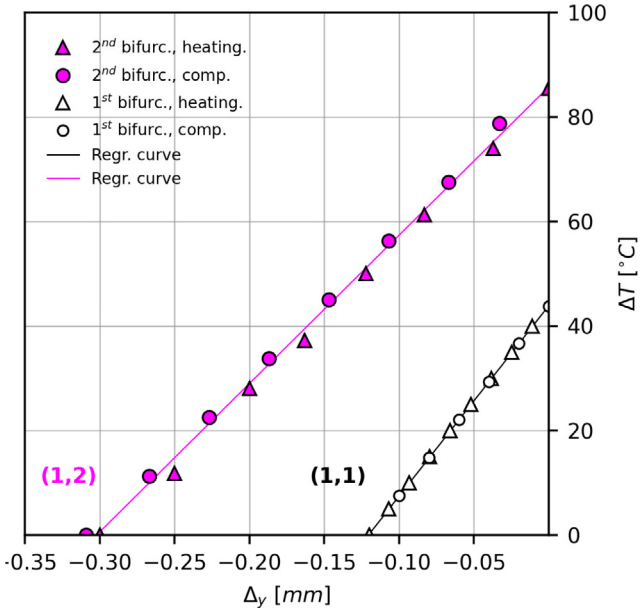

Fig. 3. FE predictions: Buckling chart for combined loading.

at position $(-0.02\ \text{mm}, 36.68°\text{C})$ using a white marker with triangular shape, as buckling was reached under heating. In an analogous manner, if an initial $\Delta T = 10°\text{C}$ is applied, buckling can be reached by applying $\Delta_{y,b1} = -0.093$ mm. The reported buckling analysis results indicate a well-defined linear decrease of buckling temperature for increasing values of loading condition Δ_y, and the same tendency manifests when the order of load application is inverted. This is in accordance with the principle of load superposition, which holds in plate linear regime, making the order of load application not relevant until the buckling load. All presented eigenvalues correspond to a $(1, 1)$ buckling shape. It can also be noted that the regression curve divides the loading diagram in two areas, corresponding to buckled and unbuckled states.

Numerical predictions for the plate post-buckling behavior obtained by dynamic explicit analysis are presented in Fig. 4(a) and (b), where two graphs for "*compression + heating*" and "*heating + compression*" load cases are reported. These graphs capture only the last loading phase. Curves for varying amounts of initial preload are reported. For instance, in Fig. 4(a) the curve labeled as $\Delta_y = -0.08$ mm indicates a displacement of −0.08 mm previous to heating phase, while in Fig. 4(b) the curve labeled as $\Delta T = 22.5°\text{C}$ represents an initial heating phase of 22.5°C. Looking now at Fig. 4(a), the "*pure heating*" case, labeled as $\Delta_y = 0.000$ mm, is the curve reaching the highest temperature. During heating phase, plate deflections are zero till a critical value of ΔT is reached and the plate starts deflecting out of plane. For a plate with no imperfections, the buckling temperature is close to the previously calculated linear eigenvalue, $\Delta T_{b1} = 43.81°\text{C}$, plotted in Fig. 3 on the vertical axis. If temperature continues rising beyond ΔT_{b1}, deflection W starts growing under a $(1, 1)$ buckling shape. When temperature reaches a value $\Delta T = 85.5°\text{C}$, the plate experiences an abrupt mode jump into a $(1, 2)$ buckling shape. The point of maximal deflection previous to the jump marks a change in slope in the curve, and is considered as the indicator of mode jump. The mode jump is registered in Fig. 4(a) as a blue triangular marker over the ΔT vertical axis, and is also reported in Fig. 3 as a magenta circular marker at $(0.00\ \text{mm}, 85.5°\text{C})$.

For increasing values of compressive preload Δ_y, the deflection curves shift downwards and mode jumping temperatures decrease: an initial amount of preload $\Delta_y = -0.04$ mm reduces the mode change temperature to $\Delta T_{b2} = 73.95°\text{C}$. Looking now at the curve for $\Delta_y = -0.120$ mm, it can be noted that deflection W is already present at $\Delta T = 0.0°\text{C}$: the Δ_y pre-load introduced during the compression phase is larger than the pure compression buckling load $\Delta_{y,b1} = -0.120$ mm, and thus buckling occurred during the first loading phase.

In an analogous manner, in Fig. 4(b) the "*pure compression*" load case is labeled as $\Delta T = 0.0°\text{C}$ and is the curve reaching the highest compressive values. At the beginning of the compression load phase, plate deflections are zero till a critical value of Δ_y is reached and out-of-plane deflections start increasing. $\Delta_{y,b1}$ is close to the ideal value for the perfect plate, given by previously calculated eigenvalue analysis $\Delta_{y,b1} = -0.120$ mm, plotted in Fig. 3. If compression increases beyond $\Delta_{y,b1}$, deflections keep growing under a $(1, 1)$ buckling shape, and, as previously seen for pure heating cases, when the compression reaches $\Delta_{y,b2}$, the plate experiences an abrupt mode jump, changing into a $(1, 2)$ buckling shape. Mode jumps can be obtained under both ε*pure heating*ε and ε*pure compression*ε load cases. The point of maximal deflection W demarcates the mode transition. The mode jump is reported in Fig. 4(b) as a magenta circular marker and is also reported in Fig. 3 at $(0.309\ \text{mm}, 0.00°\text{C})$. For increasing values of pre-heating ΔT, mode jumps appear at lower temperature. For example, an initial amount of preload $\Delta T = 22.5°\text{C}$ reduces the mode change compression to $\Delta_{y,b2} = -0.198\,\text{mm}$. Observing now the curve for preload $\Delta T = 45.0°\text{C}$, it can be noted that deflections W are already present at $\Delta_y = 0.000$ mm; this is because the Δ_y pre-load introduced during the compression phase is larger than the pure heating buckling temperature $\Delta T_{b1} = 43.81°\text{C}$, and therefore buckling occurs during the first loading phase. Reporting this, Fig. 3 is populated of magenta, circular and triangular markers which seem to be distributed approximately along a line. Performing a least square linear regression over these values reveals a well-defined linear correlation between compressive preload and mode jumps. In particular, decreasing values of initial load Δ_y decrease ΔT_{b2} in "*compression + heating*" cases, while increasing values of initial load ΔT seems to reduce Δ_y in "*heating + compression*" cases.

It is possible to note in Fig. 4(a) and (b) that the first and second bifurcations may happen during different load phases, so representing only one load phase in the diagram may leave out valuable information.

4. Test setup

The main goal of the tests is studying the buckling and mode jumping of a plate that is subjected to combinations of compressive load and heat. The test setup is shown in Fig. 5. The composite plate is bolted to a frame. The frame is made in Invar 36 material [42] which has a low CTE, see properties in Table 1. Low CTE fittings are useful for two purposes: restraining thermal expansion of the plate and reducing the chances of non-uniform compression due to irregular thermal expansion.

Prior to the testing, the composite plate is placed between the two symmetric parts of the frame. When assembled, the exterior edge of the plate remains gripped by the frame. The holes in both plate and frame are large enough to avoid contact of the bolts with the plate. The assembly is completed by following a cross-sequence to bolt the assembly in three levels up to the maximal level of 60 Nm. This torque guarantees uniform constraining of the plate in-plane displacements. The alignment of both frame parts was ensured by the use of alignment pins.

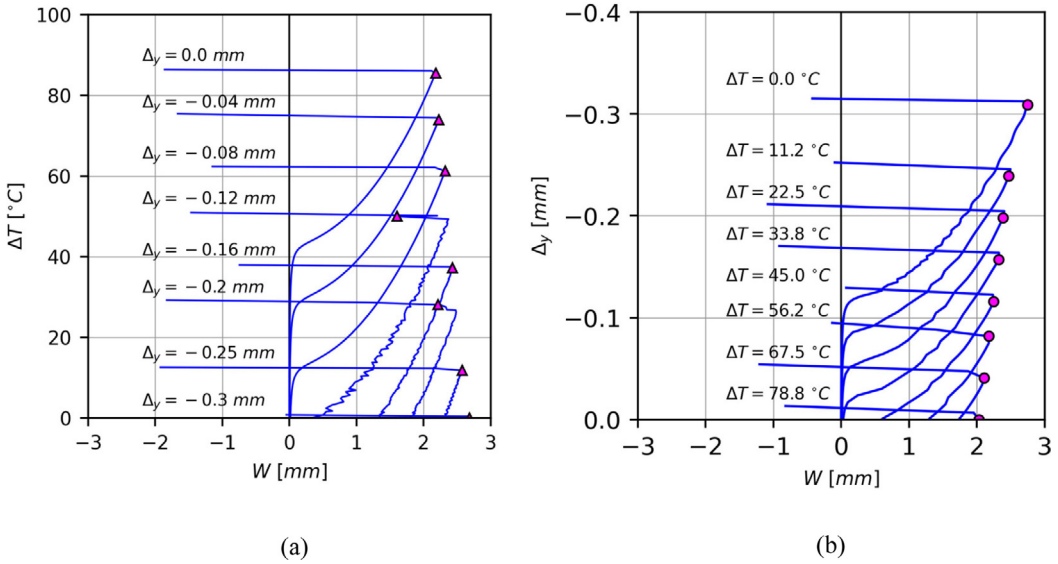

Fig. 4. FE load vs deflection curves: (a) Heating + Compression; (b) Compression + Heating.

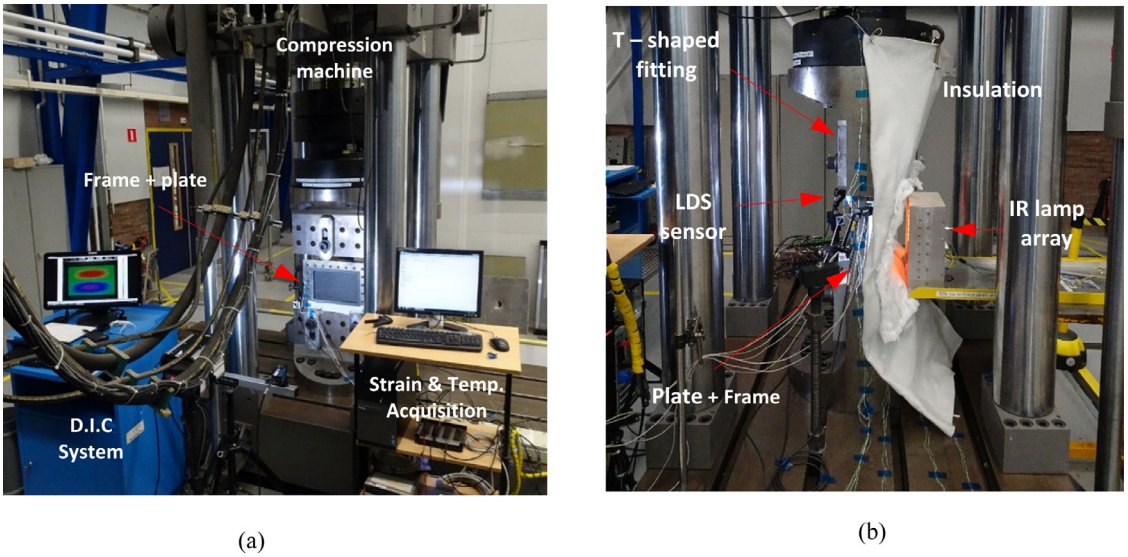

Fig. 5. Test setup: (a) Front view; (b) Side view.

The test setup is built in a compression machine, with a maximal compressive force of $3500kN$. The machine consists of a canopy structure in which four columns support a high-stiffness crosshead with adjustable height. The crosshead has an integrated load actuator and hydraulic manifold, which support the loading cylinder and a load transducer for force monitoring. The machine is equipped with an LVDT sensor that monitors the vertical displacements of the cylinder.

Six strain gauges were placed at six different positions, as shown in Fig. 6, to monitor longitudinal strain during compression tests. At positions 1 and 4, two strain gauges were placed at the front and back of the frame, labeled as "F" and "B", respectively. The gauges were connected in a half-bridge, for self-compensation of temperature. Once installed in the frame, the tested plate acquired an inherent initial imperfection, caused by the gripping surfaces and the torquing operation.

The load transfer between compression machine and frame was done through two T-shaped stainless steel fittings: they were attached to the loading cylinder and to the base of the test machine, and the invar frame was placed in-between. The load introduction process is regulated by a fully automated computer system that allows for displacement-controlled loading. Additionally, two external laser LDS sensors were used to monitor the vertical displacement of the compression fitting to account for machine compliance during testing. The FE analysis had also the function to provide estimations of maximum expected loading Δ_y. It should be clarified that the low CTE of the frame makes it less sensitive to temperature changes. Ultimately, and because the plate is attached to the frame, almost the totality of the size variation in height b experimented by the plate is originated by the compression applied to the frame and not by thermal expansion caused by heating loads.

The source used to heat the plate was an IR lamp array, shown in Fig. 6(b). It consists of eight lamps with a maximum power of $1000W$ at $200V$. The lamps were used with a power source able to deliver $120V$ and $50A$. The heat provided by the IR array was regulated by manually increasing the input power. The heat lamps were placed vertically, distributed in a $4+4$ configuration in an attempt to achieve uniform heat distribution. Temperatures were monitored with $\varepsilon K\varepsilon$ - type thermocouples in diverse positions of the setup: one measuring point for room temperature, nine measuring points on the plate, two on the T-shaped compression fittings, as reported in Fig. 6. Readings for

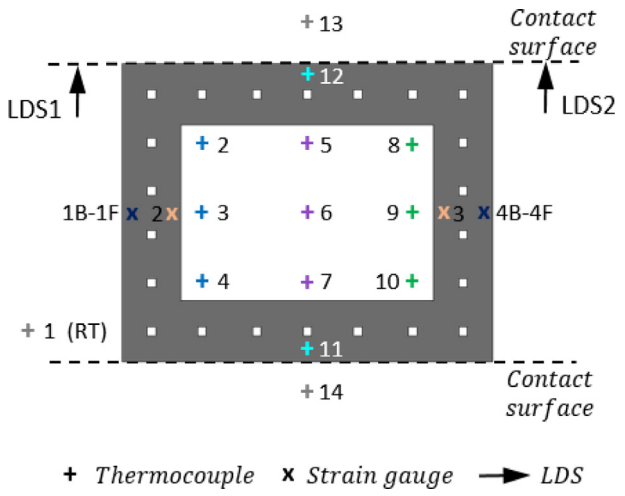

Fig. 6. Test setup: sensor distribution.

thermocouples, strain gauges, LDS lasers and load cell where simultaneously acquired by a "Keythley" multimeter. Out of plane displacements were monitored using a DIC equipment from the brand Correlated Solutions, model Vic3D; two different sets of cameras were used, with 30 mm and 50 mm objective lenses. In Fig. 5(a) it can be observed the uniform speckle distribution of white dots over black background that was applied on the plate. In order to protect the LSD laser sensors from the heat radiated by the lamps, a layer of aluminum wool was used, as shown in Fig. 5(b).

For the implementation of the four described load cases, four different testing protocols were followed. During the "*pure compression*" tests, the vertical position of the T-shaped adaptor was set to enter in contact with the frame, and the Y position of the machine was set to zero. Then, a displacement of $\Delta_y = -0.4$ mm was enforced to the frame. This was done along a period of 3 min, during which the strains in the frame were monitored, as shown in Fig. 7(a) where strains are plotted versus reaction force in the compression machine. Once reached, the maximal load is maintained for 30 s and after that gradually released. These data are used to ensure compression uniformity in the frame. Finite element simulations have also been included in the plot. It can be observed that compression is not fully uniform, as gauges $1F$ and $1B$ deliver slightly larger strains than gauges $4F$ and $4B$. An approximate difference of $60\mu\varepsilon$ between left and right sides is captured in the gauges at almost all loading states. Even though attempts were made to solve this issue, it could not be improved due to the limited adaptability of the compression head of the loading machine. This alignment error is percentage-wise larger at low compression levels, while it is smaller when the load increases. It needs to be noted that the test setup is an approximation of an ideal condition: during the experiments, plate height experiences a shortening while plate length remains constant. In reality, the compressed elements of the frame experiments a small sideways deflection: the columns experience a small lateral arching deflection, which was never larger than 0.04 mm at maximal compressive $\Delta_{y,max} = 0.4$ mm, that means, 10% of the maximal compressive $\Delta_{y,max}$. It can therefore be assumed that the effect of lateral distortion, even if present, is not dominant in the experiment.

Prior to a "*pure heating*" test, the T-shaped adaptor is set in contact with the frame as in the "*pure compression*" case, and is kept at a fixed position for the duration of the test. Once this is done, the IR lamp array is turned on, and the heating of the plate starts. This operation is performed manually, at a speed of approximately 3°C/min . Once the goal temperature is reached, the lamps are turned off and the whole setup is let to cool down. In Fig. 7(b), measurements of the thermocouples are reported. From the data collected for sensors $TC2$ to $TC10$, on the plate, a large dispersion can be observed, reaching these up to 30°C at large temperatures. Attempts were made to improve the uniformity of the temperature distributions by changing the distribution of the heat lamps, however, no improvement was achieved. It can be appreciated from the sensors $TC11$ and $TC12$ that there is a temperature gradient within the invar frame itself of approximately 23°C; but due to its low CTE the effects of this variation are non-significant. Temperatures for thermocouples $TC13$ and $TC14$, placed at the T-shaped fittings, are indistinguishable from the $TC1$, measuring room temperature, and are not reported in the graph.

The procedures followed for "*compression + heating*" and "*heating + compression*" tests keep the essence of the procedures. In the "*compression + heating*", the compression head is first adjusted to the frame, and the vertical position is set to zero. Once preload Δ_y is applied, the heat lamp array is turned on and heat is gradually applied to the specimen. When the pre-fixed goal temperature is reached, the lamps are turned off and the specimen is unloaded. Conversely, during "*heating + compression*", the position of the compression is set to zero, then heat is applied, and after a goal ΔT is reached, a fixed Δ_y compression phase, similar to the one in the "*pure compression*" test.

5. Experimental results

A total of 22 tests were conducted and a few examples of typical results for each type of performed tests are reported.

Due to asymmetries in the obtained buckling shapes, it was found convenient to monitor out-of-plane displacements W at three plate positions, referred as $P0$, $P1$ and $P2$: position $P0$ corresponds to the plate center, with coordinates $(a/2, b/2)$, and positions $P1$ and $P2$ are placed over the vertical symmetry axis of the plate, at positions $(a/2, 3b/4)$ and $(a/2, b/4)$, respectively. The graphical notation for depicting each position is the same for all experiments: deflections at $P0$ or plate center are represented by a bold continuous gray curve, while curves for points $P1$ and $P2$ are reported as dashed and dash-dotted gray bold lines, respectively.

5.1. Pure heating and pure compression load cases

Results of "*pure heating*" and "*pure compression*" loading tests are represented in Fig. 8(a) and (b). These are reported as graphs representing applied ΔT versus W and applied Δ_y versus W, respectively. Finite element simulations for both loading cases are also represented in the graphs. Regression curves and cross-shaped markers present in both figures are used for the extraction of buckling loads, and are discussed later in this section. Plots for both experimental and numerical deflection shapes are reported in Fig. 9.

For the "*pure heating*" tests, the observed behavior is in line with the numerical simulations: when ΔT is gradually applied, the plate remains flat up to the point where the buckling temperature is reached; beyond that point, the plate starts deflecting out of plane, in a $(1, 1)$ buckling shape. Out of plane deflections W have negative values, which means that the plate moves towards the heat source. Deflections W continue growing, occurring the largest plate deflections approximately at the plate center.

The obtained buckling shape is not fully symmetric, as position $P1$ reaches much larger deflections than its counterpart $P2$; however, a $(1, 1)$ mode is clearly predominant, as seen in Fig. 9(a). If ΔT keeps increasing, the current buckling shape abruptly changes its shape into a $(1, 2)$ buckling mode at around $\Delta T_{b2} = 80.0$°C. At that moment, deflections at $P0$ shift towards zero, as this point changes from having nearly maximal plate deflections to be in the proximity of a nodal line of the new buckling shape with almost zero deflections. Plate behavior is comparable to numerical predictions, even though buckling happened much earlier than the predicted $\Delta T_{b1} = 43.81$°C, and the numerical mode jump happened at $\Delta T_{b2} = 85.81$°C. FE predicted deflection shapes deliver reasonably well with experimental results, as shown in Fig. 9(a).

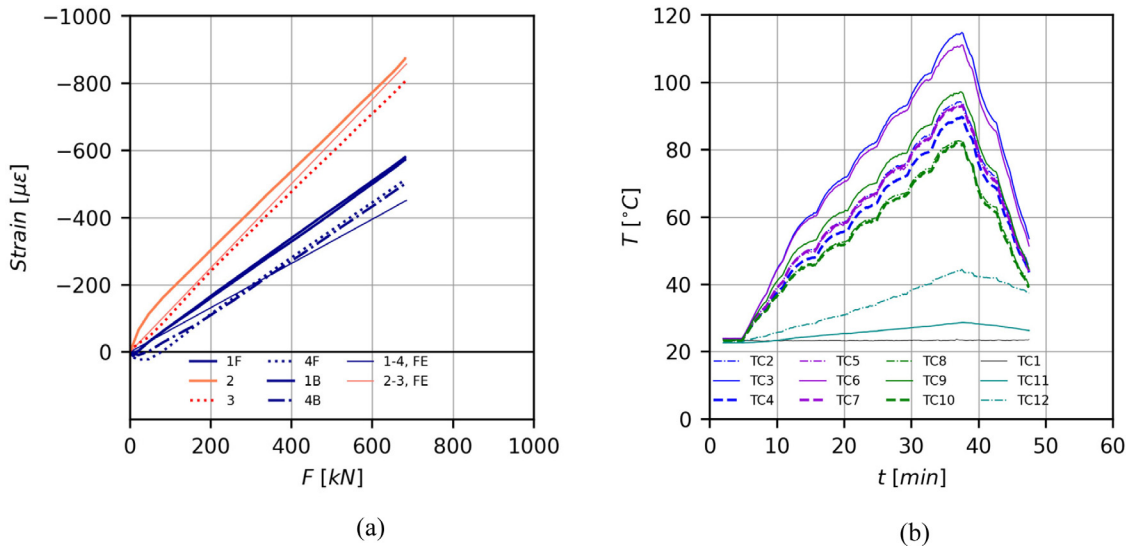

Fig. 7. Example of sensor measurements: (a) Strain gauges in pure compression test; (b) Thermocouples in pure heating test.

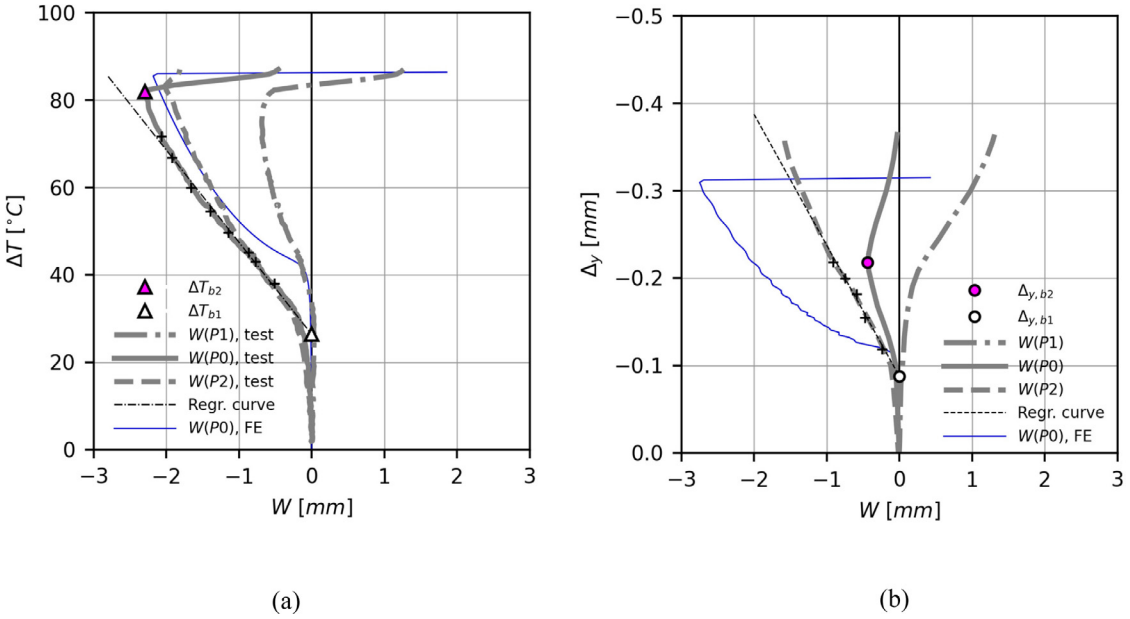

Fig. 8. Test results: (a) Pure heating case; (b) Pure compression case.

For the *"pure compression"* test, differences can be noted with respect to the heating case. When compression loads were applied, plate displacements slowly increased up to a point where they started growing faster and the plate could be considered as buckled. Maximal deflections were not reached at the plate center, but at both $P1$ and $P2$ positions, as shown in Fig. 9(b). The asymmetry of the initial buckling shape was much more pronounced than in pure heating tests. Out-of-plane displacements started happening much earlier at $P2$, than at $P1$ or at the plate center $P0$. The obtained buckling shape resembles a $(1,2)$ mode where one of the half-waves is much larger than the other. This is consistent with previously shown results for pure heating tests, where $P2$ deflections were consistently much larger than at its symmetric counterpart $P1$. When load kept increasing, deflections at $P0$ and $P2$ kept growing up to a point where $P0$ finds a maximum value; after that point, deflection in the plate center started decreasing till it went to zero, and deflections at $P1$ started to grow, gradually shifting into a fully developed $(1,2)$ mode. Also, clear differences can be observed with the numerical simulation: even if the simulation appears to capture well the buckling onset, the test showed a progressive transition into $(1,2)$ mode rather than an abrupt change.

Even though pure heating and pure compression tests showed clear differences in their buckling shapes, there are similarities between them. For both experiments, the half-wave showing maximal deflections at buckling is not in the center of the plate, but rather displaced towards plate position P2.

Choosing criteria for the identification of bifurcation points is a challenging task. For comparability, these criteria need to be applicable to all four types of performed tests.

First, defining buckling in a plate is not a evident occurrence, as plates do not show a clear behavior at buckling onset. A classical way to perform this operation is using so-called "direct" methods [43], where the critical buckling load is extracted from a test output curve such as "load versus out-of-plane deflection" or "load versus strain". The buckling load can be then determined in two ways: automatically assigning buckling to a recognizable point in the curve, such as a slope or a curvature change, or performing a fitting curve/regression curve

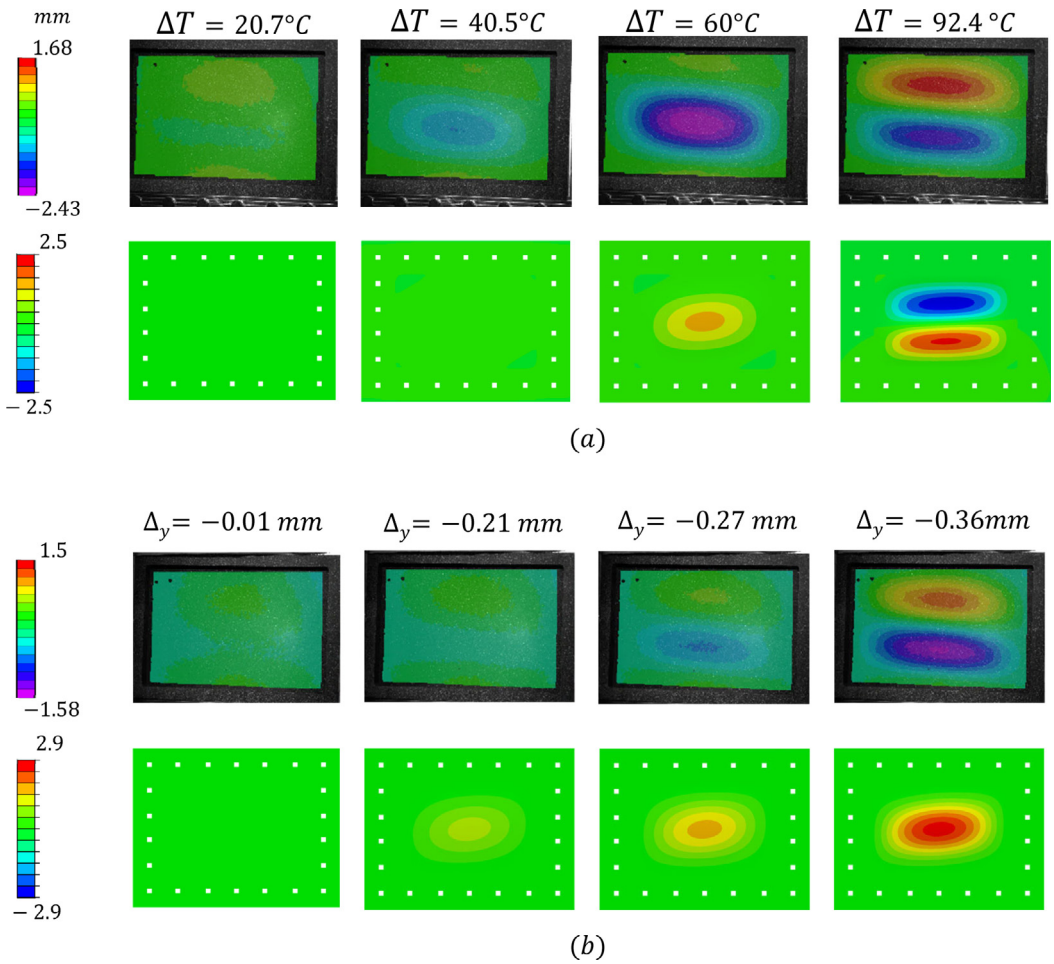

Fig. 9. Experimental and numerical deflection shapes: (a) Pure heating; (b) Pure compression.

over points in the stable post-buckling region. The buckling load is then assigned to the intersection of this regression curve with the load vertical axis.

Regarding the identification of a mode jump, it can be easier when it happens suddenly, such as in a typical pure heating test, while it can be more unclear when it happens gradually, as in a pure compression test. Methods available in literature involve monitoring plate strains at certain plate positions, using back-to-back strain gauges, but due to the chosen sensor layout this methodology cannot be applied.

Thus, two methodologies for the identification of bifurcations are here presented. For the extraction of buckling bifurcation points, a method referred as "*load vs. displacement*" is used: from the three deflection curves at $P0$-$P1$-$P2$ positions, the one showing highest deflections is selected; points from the deep post-buckling are chosen and then a least-square linear fitting is performed over them. The plate is considered buckled at the load value at which the regression line intersects the vertical axis. An example can be seen in Fig. 8(a) and (b), where selected points are reported as black markers with a "+" shape. These points should be located at the stable post-buckling range and at a loading state inferior to the second bifurcation load, as curve stiffness varies after mode change. For instance, in Fig. 8(a) the method is applied on the curve $P0$ yielding $\Delta T_{b1} = 27°\text{C}$, while in Fig. 8(b) the method is applied at $P1$ and yields a $\Delta_{y,b1} = -0.093$ mm. The obtained bifurcation points are registered in Fig. 8(a) and (b) as white markers, with triangular shape for the "*pure heating*" test, and circular shape for the "*pure compression*" test.

For the extraction of mode jump bifurcations, a method referred as "*slope vs. displacement*" is proposed. This method relies on the fact that during the test, deflections W at plate center increase till the moment when a mode change happens, and then they go back to zero, as position $P0$ is close to a nodal position in the new $(1,2)$ buckling configuration. The point of maximal W, that marks a change in slope sign, is used here to mark the transition into the $(1,2)$ mode. This transition may either be sudden, such as in Fig. 8(a), or a gradual change, as in Fig. 8(b). The result of applying this methods yields $\Delta T_{b2} = 82°\text{C}$ for the "*pure heating*" case, and $\Delta_{y,b2} = -0.22$ mm for the "*pure compression*" case. These new bifurcation points are reported in Fig. 8(a) and (b) as magenta colored markers, with either circular or triangular shape depending on loading condition acting at the moment of bifurcation.

For any performed test, either pure or combined, the obtained bifurcation points can be documented in an overview chart such as Fig. 10, where load condition ΔT is plotted versus applied Δ_y. Fig. 10 contains an overview of all experiments performed in this campaign: two clouds of colored markers are reported, corresponding to buckling and mode jumping bifurcations. For the tests presented in this section, only one load type was applied, and therefore their bifurcation points lay approximately along the axis lines, i.e. X axis for pure compression and Y axis for pure heating tests, respectively. Thus, for the pure compression test, two bifurcation points, labeled as $PC01$ are reported at $(-0.091\text{ mm}, 0.0°\text{C})$ and $(-0.220\text{ mm}, 0.0°\text{C})$, and are reported as white and magenta circular markers. In the same way, for the pure heating test two triangular, white and magenta colored markers labeled as $PH01$ are registered at locations $(0.000\text{ mm}, 27.0°\text{C})$ and $(0.000\text{ mm}, 82.0°\text{C})$.

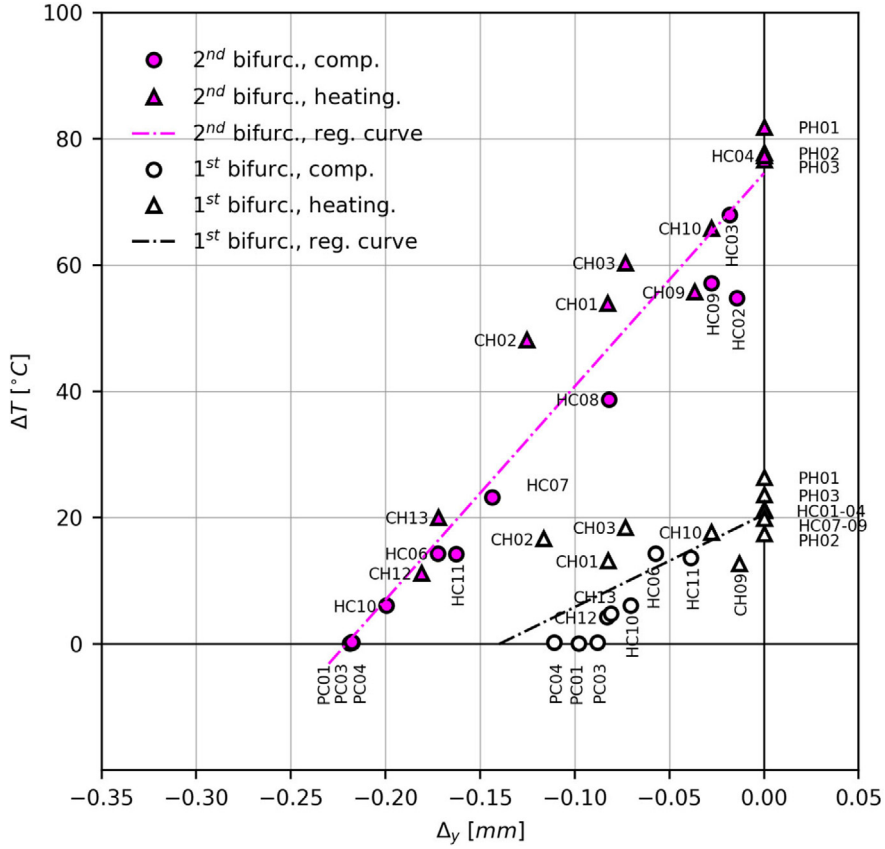

Fig. 10. Experimental buckling chart.

5.2. Combined load cases

Fig. 11(a) and (b) represent two examples of "$compression + heating$" combined test. Each graph is divided in two halves where the lower and upper parts represent the first and second loading phases, respectively. The plate deflections at the end of the first load phase are the initial deflections for the second load phase. It can be observed how the test in Fig. 11(a) begins with an initial compression load of $\Delta_y = -0.028$ mm, while the preload in Fig. 11(b) is equal to $\Delta_y = -0.0821$ mm. Once the entire compression load is applied, the lamps are turned on and the plate is heated up to $\Delta T = 80.00°C$ in both cases.

It can be seen that for both tests, the plate remained flat during the compression phase and started deflecting during the heating phase. Thus, buckling and mode change bifurcations take place during the heating phase and the corresponding markers are located in the upper half of the diagram. For the first test, which results are reported in Fig. 11(a), $\Delta T_{b1} = 17.69°C$ is found, while lower $\Delta T_{b1} = 13.1°C$ is found for the second test, recorded in Fig. 11(b). Values of $\Delta T_{b2} = 65.8°C$ and $\Delta T_{b2} = 53.9°C$ are found, respectively. Plate deflections show a clear resemblance with pure heating tests. The effect of preload is evident as ΔT_{b1} and ΔT_{b2} have decreased with respect to the pure heating test. This tendency becomes more evident for increasing values of preload Δ_y. The maximal deflections W decrease with Δ_y, and the trajectories followed by the three control points $P0$, $P1$ and $P2$ come to resemble more those observed in "pure compression" cases.

In Fig. 12(a)–(d), four examples of "$Heating + Compression$" experiments are reported. These four experiments were performed sequentially. In all of them the same procedure was followed: First, the plate is heated up to a given temperature, reaching a loading state $(0, \Delta T)$; this process is from now on referred as "heating phase". Second, a compression load Δ_y is applied on top, reaching a loading state $(\Delta_y, \Delta T)$; after that, the load Δ_y is retired, returning to loading state $(0, \Delta T)$; the operation of applying and removing Δ_y is referred as "compression phase". Subsequently, the plate is heated to a higher value of ΔT and the compression procedure is repeated. It was found that independent of the amount of preload ΔT, in every case, the plate returned to the buckling configuration before the compression Δ_y was applied. This occurrence was found to be consistent and repeatable. The starting ΔT of these compression phases can be identified at the lower part of graphs while the evolution of the plate deflections can be followed in the upper part. It can also be seen that the initial deflections for each one of these compression phases increases with the applied ΔT. DIC deflection shapes are reported in Fig. 13 for each one of these compression phases.

The first compression phase is documented in Fig. 12(a) and in the upper row of images in Fig. 13. First, temperature is increased and stabilized at $\Delta T = 14.3°C$, and then a compression phase is applied. The starting point of the compression phase is registered in the bottom part of the graph as a blue square dot. The compression phase can be followed in the upper part of the graph, where deflections continue to grow for increasing values of loading condition Δ_y. During this loading phase the plate finds both buckling and mode change bifurcations, registered in the graph as white and magenta circular markers at $\Delta_{y,b1} = -0.057$ mm and $\Delta_{y,b2} = -0.172$ mm. In Fig. 13, obtained deflections shapes show how at $\Delta_y = -0.100$ mm a mild (1,2) mode is present, while at $\Delta_y = -0.175$ mm, a (1,2) shape can be appreciated and at $\Delta_y = -0.300$ mm a fully developed $(1, 2)$ mode is clearly identifiable. The two obtained bifurcation points are then registered in Fig. 10 at positions $(-0.057 \text{ mm}, 14.3°C)$ and $(-0.172 \text{ mm}, 14.3°C)$ respectively, both of them labeled as $HC06$. As both bifurcations happen during the same loading phase, both points are located over the same isothermal line. Once the load Δ_y is retired, the plate returns to its initial (1,1) shape.

For the second compression test, the heating phase is documented in Fig. 12(b) and in the second row of images in Fig. 13. Prior to compression, the temperature is first risen from $\Delta T = 14.3°C$ up to $\Delta T =$

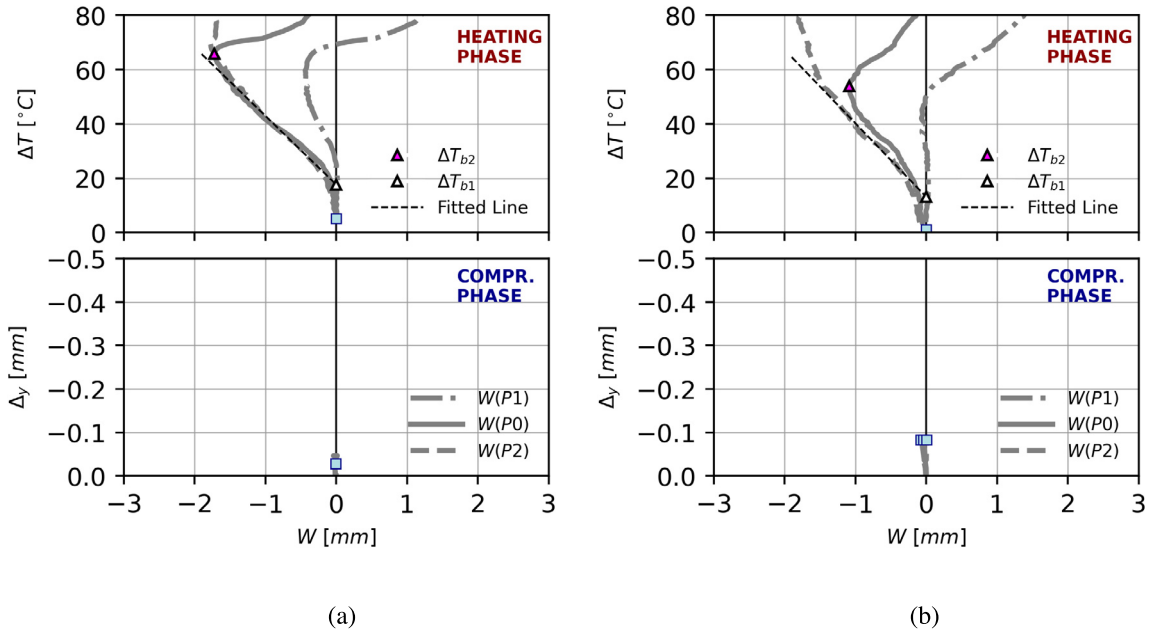

Fig. 11. Test results for "Compression + Heating" case: (a) $\Delta_y = -0.028$ mm; (b) $\Delta_y = -0.081$ mm.

23.23°C, and then a new compression phase is applied. The first bifurcation is reached during the new heating phase, at $\Delta T_{b1} = 12.15$°C, and it is reported in the lower part of the figure as a triangular white marker. However, there are still not enough points in the post-buckling region and this prediction is still unreliable The second bifurcation is reached during the compression phase at $\Delta_{y,b2} = -0.144$ mm, and it is registered as a magenta circular marker in the upper part of the diagram. DIC plots at Fig. 13 show how for temperature values of $\Delta T = 23.23$°C, mild deflections are already present for $\Delta_y = -0.010$ mm, and how the switch into a (1,2) shape starts happening already at $\Delta_y = -0.100$ mm. The effect of the initial ΔT manifests in the earlier occurrence of bifurcation points. Second bifurcation point is also registered in the buckling chart in Fig. 10, at position $(-0.144\text{ mm}, 23.23°\text{C})$ labeled as $HC07$ with a magenta circular marker. After the load decreases, the plate returns back to (1,1) mode.

Results for the third compression phase are reported in Fig. 12(c) and in the third row of Fig. 13. The compression cycle is performed after temperature is increased from $\Delta T = 23.23$°C to $\Delta T = 38.54$°C. A linear regression can now yield much more reliable results for buckling. Indeed, the regression yields a ΔT_{b1} equal to 19.85°C. Mode change is reached under compression at $\Delta_{y,b2} = -0.082$ mm, and is then registered in Fig. 10 at position $(-0.082\text{ mm}, 38.71°\text{C})$, labeled as $HC08$. In the DIC plots it can be seen that the mode change happens at even smaller values than at previous compression phases.

For the fourth and last compression phase results are reported in Fig. 12(d) and in the fourth row of DIC images in Fig. 13. It can be observed that the buckling shape for $\Delta_y = -0.01$ mm is a fully developed $(1,1)$ mode with the crest peak slightly off the plate center. As soon as compression phase starts, deflections at point $P0$ start decreasing very fast, instead of decreasing gradually like in previous compression phases. Then, the plate remains at a (1,2) mode shape indefinitely as long as ΔT is maintained. The second bifurcation is then assigned to $(-0.028\text{ mm}, 57.12°\text{C})$, reported in Fig. 10 as $HC09$.

An overview of all performed experiments can be observed in Fig. 10, where two clouds of colored markers are reported, corresponding to buckling and mode jumping bifurcations. Linear regressions for both point clouds, performed using the "least squares" procedure, are reported as dot-dashed lines in the graph. A Pearson correlation for both point clouds yields R factors of 0.793 for the buckling bifurcation cloud points and 0.967 for the cloud of mode jumping points. It can be concluded that linear relation between Δ_y and ΔT is well defined for buckling bifurcation and very good for the mode change bifurcations. These lines confirm the tendencies predicted by the numerical analysis, also for the mode change bifurcations. For pure heating and pure compression cases, the dispersion among bifurcation points is larger for buckling than for the mode jumping temperatures. The bifurcation points reached under compression are mostly below their corresponding regression lines, while bifurcation points reached under heating are mostly placed above them. Besides, buckling values show large dispersions for all tested load combinations, while for mode jumping large dispersion happens at large temperatures and decreases almost totally for pure compression cases. It is believed this occurrence is caused by the gradients in the plate at high temperatures, documented in Fig. 7(b).

In Fig. 14, experimental regression lines are plotted against numerical predictions: two lines representing the regression curves from FE simulations are reported as thin continuous lines, while experimental regressions are represented as dot-dashed lines. Large differences on the magnitude of the buckling loads can be observed: all experimental values are significantly lower than their numerical counterparts. In the pure compression, predictions appear to underestimate compression buckling loads, while in pure heating predictions appear to overestimate them. For mode jumping values, FE simulations are consistently higher than their experimental counterparts, being the differences larger for values with a higher compressive component.

One of the principal sources of discrepancy respect to the behavior of an ideal plate in any buckling test are the initial imperfections. In Fig. 15, the typical imperfection shape measured during the test campaign is reported. The measured imperfections, consistent throughout all tests, had one fully developed half-wave in the upper half of the plate, while in the lower half, a second half-wave and a partially developed third half-wave along the Y axis can be appreciated. It can also be noticed an area in the upper left and right corners of the plate with a negative value, while in the upper horizontal edge between the two corners it is positive. This means that the upper horizontal edge of the plate was slightly bent outwards. The imperfection had a maximal amplitude of 20% of plate thickness, however the shape was highly distorted. Such initial shape would explain the consistent tendency in compression dominated tests to almost skip the $(1,1)$ buckling shape and go directly into a $(1,2)$ shape. This imperfection was probably originated during

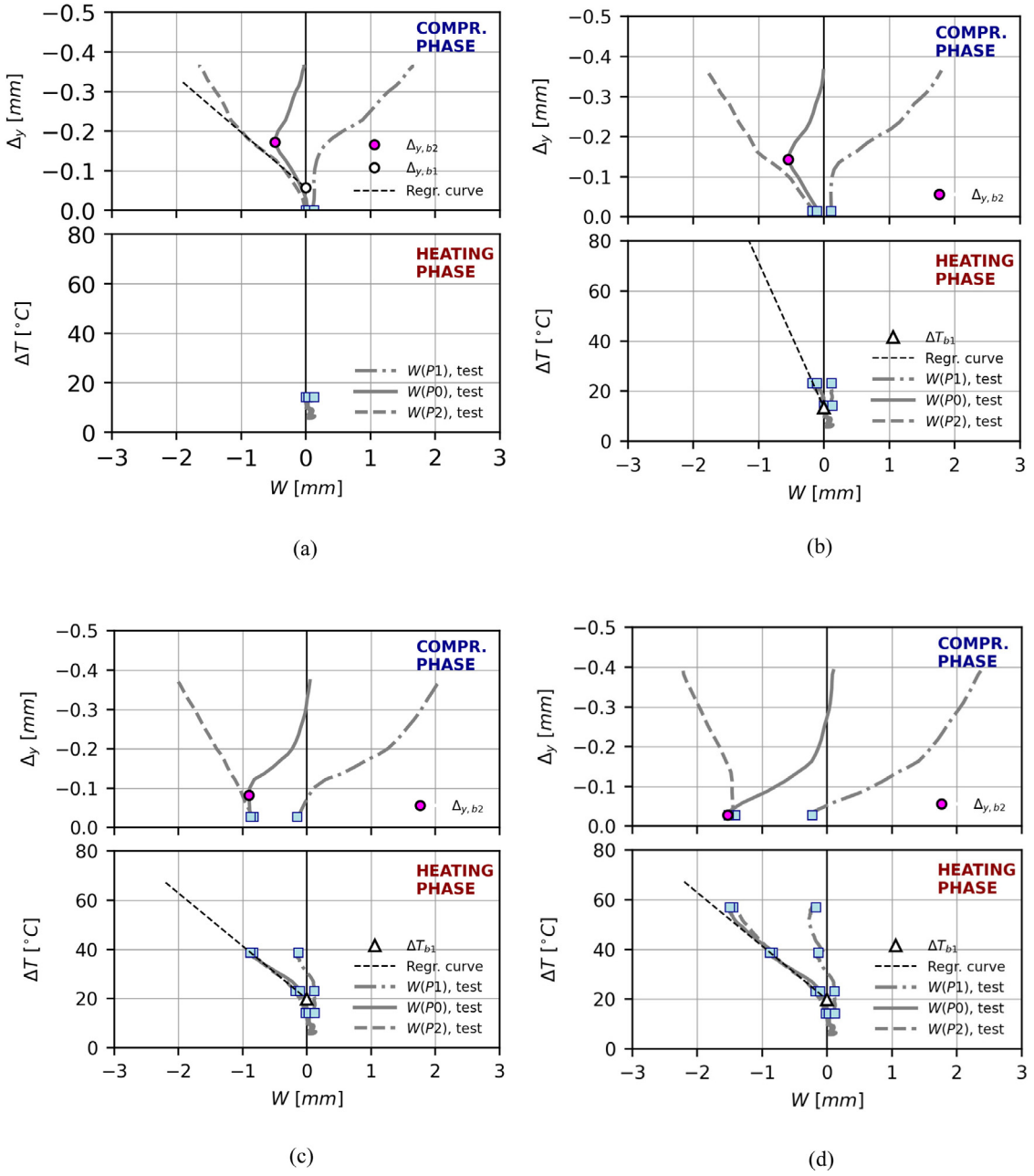

Fig. 12. Test results for "Heating + Compression" cases: (a) $\Delta T = 14.3°C$; (b) $\Delta T = 23.1°C$; (c) $\Delta T = 38.5°C$; (d) $\Delta T = 56.9°C$.

the assembly operation of the frame: torquing the frame could yield an initial out-of-plane deformation due to the squeezing of the plate and related Poisson's transverse effects, or due to irregular application of torque. Initial imperfections, however, are only one of the multiple reasons for divergence. Differences between experimental results and numerical predictions could have also been originated by other sources: variability of material properties, change of material properties due to heating, through-thickness temperature gradients and non-uniform in-plane temperature distributions, differences in temperatures between frame and specimen. The quality of the predictions could be improved by separately tacking any of these potential discrepancy sources.

Even though the setup can certainly benefit from refinement in some aspects of its design, such as compression uniformity or improvement in temperature distributions, insight about the interaction of mechanical and thermal loads was gained. Several phenomena were successfully captured experimentally: decreases in both buckling and mode jumping loads were successfully captured for different amounts of pre-load; and it was also found that in *"heat + compression"* load cases, the mode jump was reversible once the mechanical load decreased. This experimental work contributes to expand previous gained experimental knowledge about mode jumps in heated composite plates [8]. Better understanding on the appearance of mode jumps plates under heat and compression could be valuable knowledge for future designs when considering aerospace components operating in thermomechanical post-buckling regime, as well as for future research fields such as morphing, as mode jumps in composite plates could potentially be used as a source for shape change.

6. Conclusions

During this research, the buckling and mode jumping behavior of thermally and mechanically loaded composite plates was studied. A novel experimental setup for combined tests was proposed. The setup is conceived around a frame with a low coefficient of thermal expansion,

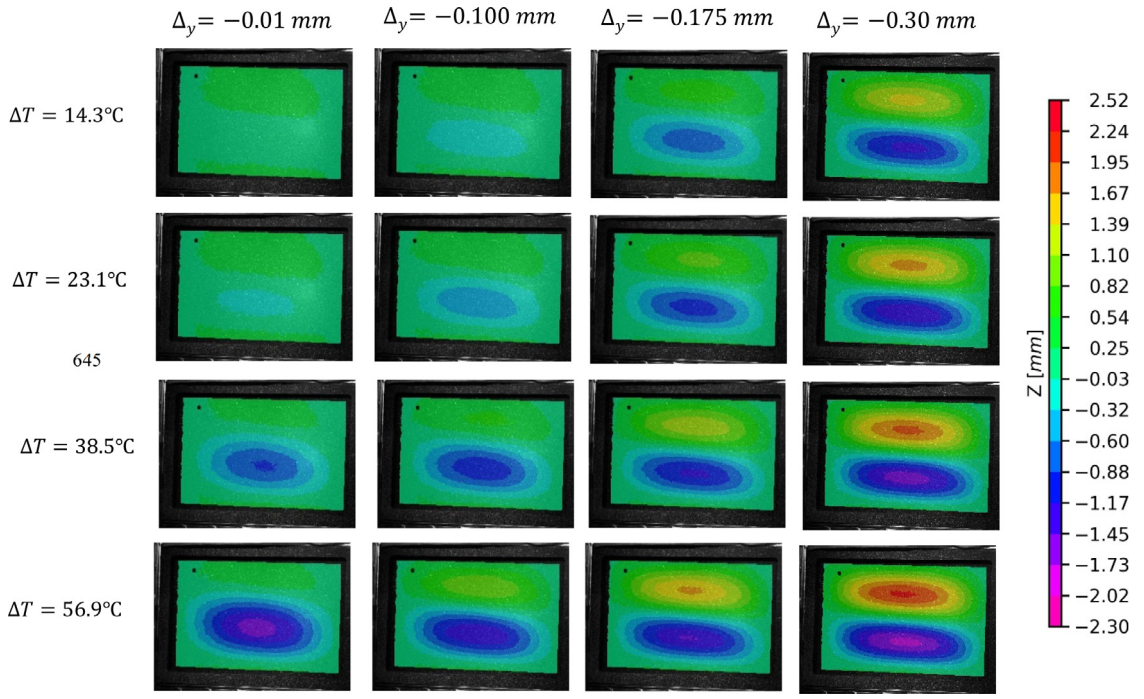

Fig. 13. Experimental deflection shape under combined loading.

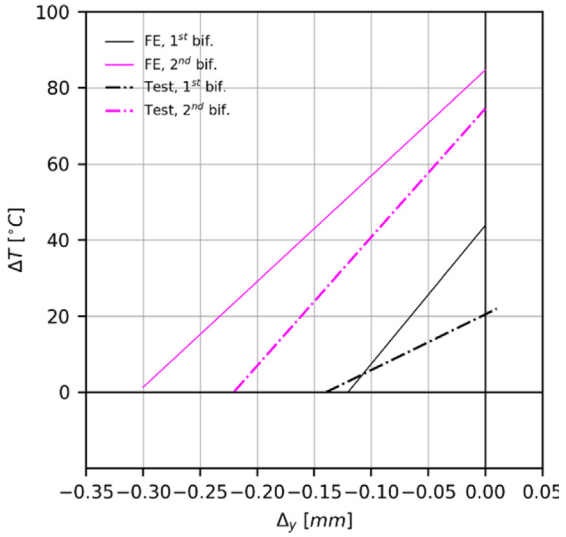

Fig. 14. Comparison between experimental results and numerical predictions.

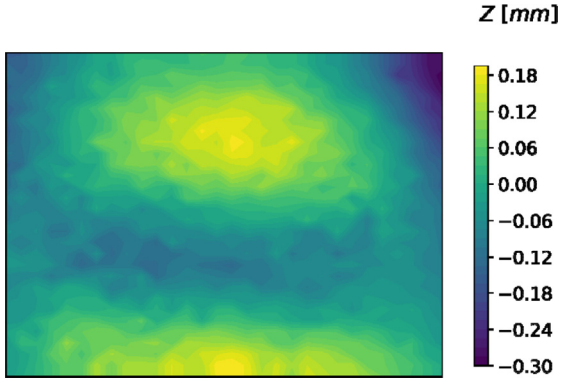

Fig. 15. Measurement of initial imperfections in the plate.

so that the plate can experience buckling and mode jumping when heated, and also when subjected to mechanical load by compressing the frame. Experimental results were delivered as load vs out-of-plane deflection graphs, deflection plots and an overview buckling chart in the form of temperature variation ΔT vs. displacement Δ_y. Even if there are differences between experimental results and numerical predictions, the finite element analysis managed to anticipate the most critical trends. Reported data appear to confirm a linear relation between the two loading conditions ΔT and Δ_y for the mode jumping bifurcations. However, for the occurrence of buckling the same linear tendency could not be confirmed, even if the results are encouraging of the existence of such trend. Potential sources of difference between numerical and experimental data are the variability of plate geometrical imperfections, irregularity in temperature distributions and potential changes in material properties. These experimental results are still, however, preliminary, and should be seen as a proof of concept. It is expected this research to contribute to the extension of the operative range of composite panels into the thermomechanical post-buckling regime, as well as open the door for potential passive, heat/compression-triggered shape change of aircraft composite thin structures.

CRediT authorship contribution statement

Javier Gutiérrez Álvarez: Conceptualization, Methodology, Software, Validation, Formal analysis, Investigation, Data curation, Writing – original draft, Writing – reviewing & editing. **Chiara Bisagni:** Conceptualization, Supervision, Writing – reviewing & editing, Funding acquisition.

Declaration of competing interest

The authors declare that they have no known competing financial interests or personal relationships that could have appeared to influence the work reported in this paper.

References

[1] J. Williams, M. Stein, Buckling behavior and structural efficiency of open-section stiffened composite compression panels, in: 17th Structures, Structural Dynamics, and Materials Conference, 1976, p. 1727, http://dx.doi.org/10.2514/6.1976-1727.

[2] S.Y. Kuo, Flutter of thermally buckled angle-ply laminates with variable fiber spacing, Composites B 95 (2016) 240–251, http://dx.doi.org/10.1016/j.compositesb.2016.04.009.

[3] W.L. Ko, Thermal analysis stiffened and mechanical buckling of hypersonic aircraft panels with varying hat-face sheet geometry and fiber orientation, NASA Tech. Memo. 4770, 1996, https://ntrs.nasa.gov/citations/19970005336.

[4] J. Lee, M. Bhatia, Impact of corrugations on bifurcation and thermoelastic responses of hat-stiffened panels, Thin-Walled Struct. 140 (2019) 209–221, http://dx.doi.org/10.1016/j.tws.2019.03.027.

[5] P.M. Reis, A perspective on the revival of structural (in) stability with novel opportunities for function: from buckliphobia to buckliphilia, J. Appl. Mech. 82 (2015) http://dx.doi.org/10.1115/1.4031456.

[6] N. Hu, R. Burgueño, Buckling-induced smart applications: recent advances and trends, Smart Mater. Struct. 24 (2015) 063001, http://dx.doi.org/10.1088/0964-1726/24/6/063001.

[7] A.R. Champneys, T.J. Dodwell, R.M.J. Groh, G.W. Hunt, R.M. Neville, A. Pirrera, A.H. Sakhaei, M. Schenk, M.A. Wadee, Happy catastrophe: recent progress in analysis and exploitation of elastic instability, Front. Appl. Math. Stat. 5 (2019) 1–30, http://dx.doi.org/10.3389/fams.2019.00034.

[8] J. Gutiérrez Álvarez, C. Bisagni, A study on thermal buckling and mode jumping of metallic and composite plates, Aerospace 8 (2021) 56, http://dx.doi.org/10.3390/aerospace8020056.

[9] J. Gutiérrez Álvarez, C. Bisagni, Closed-form solutions for thermomechanical buckling of orthotropic composite plates, Compos. Struct. 233 (2020) 111622, http://dx.doi.org/10.1016/j.compstruct.2019.111622.

[10] J.N. Kotanchik, A.E. Johnson, R.D. Ross, Rapid radiant heating tests of multiweb beams, NACA Tech. Note 3474, 1956, https://ntrs.nasa.gov/citations/19930084251.

[11] R.R. Heldenfels, W.M. Roberts, Experimental and Theoretical Determination of Thermal Stresses in a Flat Plate, Langley Field, Virginia, 1952, https://ntrs.nasa.gov/citations/19930081138.

[12] K.D. Murphy, D. Ferreira, Thermal buckling of rectangular plates, Int. J. Solids Struct. 38 (2001) 3979–3994, http://dx.doi.org/10.1016/S0020-7683(00)00240-7.

[13] J.F. Rakow, A.M. Waas, Thermal buckling of metal foam sandwich panels for convective thermal protection systems, J. Spacecr. Rockets 42 (2005) 832–844, http://dx.doi.org/10.2514/1.9741.

[14] M. Amabili, M.R.S. Tajahmadi, Thermal post-buckling of laminated and isotropic rectangular plates with fixed edges: Comparison of experimental and numerical results, Proc. Inst. Mech. Eng. C 226 (2012) 2393–2401, http://dx.doi.org/10.1177/0954406211434496.

[15] Y. Xu, S. Ren, W. Zhang, Z. Wu, W. Gong, H. Li, Study of thermal buckling behavior of plain woven C/SiC composite plate using digital image correlation technique and finite element simulation, Thin-Walled Struct. 131 (2018) 385–392, http://dx.doi.org/10.1016/j.tws.2018.07.023.

[16] E.A. Thornton, M.F. Coyle, R.N. McLeod, Experimental study of plate buckling induced by spatial temperature gradients, J. Therm. Stresses 17 (1994) 191–212, http://dx.doi.org/10.1080/01495739408946255.

[17] D.A. Ehrhardt, L.N. Virgin, Experiments on the thermal post-buckling of panels, including localized heating, J. Sound Vib. 439 (2019) 300–309, http://dx.doi.org/10.1016/j.jsv.2018.08.043.

[18] V. Bhagat, P. Jeyaraj, Experimental investigation on buckling strength of cylindrical panel: Effect of non-uniform temperature field, Int. J. Non-Linear Mech. 99 (2018) 247–257, http://dx.doi.org/10.1016/j.ijnonlinmec.2017.12.005.

[19] B. Ross, N.J. Hoff, W.H.H. Horton, The buckling behavior of uniformly heated thin circular cylindrical shells, Exp. Mech. 6 (1966) 529–537, http://dx.doi.org/10.1007/BF02327232.

[20] M.S. Anderson, M.F. Card, Buckling of ring-stiffened cylinders under a pure bending moment and a nonuniform temperature distribution. NASA Tech. Note D-1513. https://ntrs.nasa.gov/citations/19630000305.

[21] B. Ross, J. Mayers, A. Jaworski, Buckling of thin cylindrical shells heated along an axial strip, Exp. Mech. 5 (1965) 247–256, http://dx.doi.org/10.1007/bf02327148.

[22] D. Bushnell, S. Smith, Stress and buckling of nonuniformly heated cylindrical and conical shells, AIAA J. 9 (1971) 2314–2321, http://dx.doi.org/10.2514/3.6515.

[23] Y. Frum, M. Baruch, Buckling of cylindrical shells heated along two opposite generators combined with axial compression, Exp. Mech. 16 (1976) 133–139, http://dx.doi.org/10.1007/BF02321107.

[24] J. Ari-Gur, M. Baruch, J. Singer, Buckling of cylindrical shells under combined axial preload, nonuniform heating and torque, Exp. Mech. 19 (1979) 406–410, http://dx.doi.org/10.1007/BF02324506.

[25] W. Percy, R. Fields, Buckling analysis and test correlation of hat stiffened panels for hypersonic vehicles, in: 2nd International Aerospace Planes Conference, American Institute of Aeronautics and Astronautics, Reston, Virginia, 1990, http://dx.doi.org/10.2514/6.1990-5219.

[26] R.C. Thompson, W.L. Richards, Thermal-structural panel buckling tests, NASA Tech. Memo. 104243, 1991, https://ntrs.nasa.gov/citations/19920006186.

[27] R.A. Fields, W.L. Richards, M.V. DeAngelis, Combined loads test fixture for thermal-structural testing of aerospace vehicle panel concepts, NASA Tech. Memo. TM-2004-212039, 2004, https://ntrs.nasa.gov/citations/20040031531.

[28] M. Rouse, D. Jegley, Testing a multi-bay box subjected to combined loads, in: C. Sciammarella, J. Considine, P. Gloeckner (Eds.), Experimental and Applied Mechanics, Vol. 4, in: Conference Proceedings of the Society for Experimental Mechanics Series, Springer, Cham, 2016, http://dx.doi.org/10.1007/978-3-319-22449-7_21.

[29] N.L. Breivik, M.W. Hyer, Buckling and postbuckling behavior of curved composite panels due to thermal and mechanical loading, J. Reinf. Plast. Compos. 17 (1998) 1292–1306, http://dx.doi.org/10.1177/073168449801701404.

[30] C. Bisagni, P. Cordisco, An experimental investigation into the buckling and post-buckling of CFRP shells under combined axial and torsion loading, Compos. Struct. 60 (2003) 391–402, http://dx.doi.org/10.1016/S0263-8223(03)00024-2.

[31] C. Bisagni, C. Walters, Experimental investigation of the damage propagation in composite specimens under biaxial loading, Compos. Struct. 85 (2008) 293–310, http://dx.doi.org/10.1016/j.compstruct.2007.10.029.

[32] C. Bisagni, G. Sala, Buckling and shape control of composite laminates using embedded shape memory alloys wires, in: Collect. Tech. Pap. - AIAA/ASME/ASCE/AHS/ASC Struct. Struct. Dyn. Mater. Conf., American Institute of Aeronautics and Astronautics, Reston, Virigina, 2004, pp. 1515–1529, http://dx.doi.org/10.2514/6.2004-1648.

[33] K.K. Shukla, Y. Nath, Analytical solution for buckling and post-buckling of angle-ply laminated plates under thermomechanical loading, Int. J. Non-Linear Mech. 36 (2001) 1097–1108, http://dx.doi.org/10.1016/S0020-7462(00)00074-3.

[34] F. Alijani, M. Amabili, Non-linear dynamic instability of functionally graded plates in thermal environments, Int. J. Non-Linear Mech. 50 (2013) 109–126, http://dx.doi.org/10.1016/j.ijnonlinmec.2012.10.009.

[35] S. Faghfouri, F.G. Rammerstorfer, Mode transitions in buckling and post-buckling of stretched-twisted strips, Int. J. Non-Linear Mech. 127 (2020) 103609, http://dx.doi.org/10.1016/j.ijnonlinmec.2020.103609.

[36] Y. Kiani, Axisymmetric static and dynamics snap-through phenomena in a thermally postbuckled temperature-dependent FGM circular plate, Int. J. Non-Linear Mech. 89 (2017) 1–13, http://dx.doi.org/10.1016/j.ijnonlinmec.2016.11.003.

[37] M. Stein, The Phenomenon of Change in Buckle Pattern in Elastic Structures, NASA Technical Report R-39, 1959.

[38] W.J. Supple, Changes of wave-form of plates in the post-buckling range, Int. J. Solids Struct. 6 (1970) 1243–1258, http://dx.doi.org/10.1016/0020-7683(70)90100-9.

[39] F. Stoll, Analysis of the snap phenomenon in buckled plates, Int. J. Non-Linear Mech. 29 (1994) 123–138, http://dx.doi.org/10.1016/0020-7462(94)90031-0.

[40] B. Falzon, G.P. Steven, Buckling mode transition in hat-stiffened composite panels loaded in uniaxial compression, Compos. Struct. 37 (1997) 253–267, http://dx.doi.org/10.1016/S0263-8223(97)80017-7.

[41] M. Cerini, B. Falzon, Use of the arc-length method for capturing mode jumping in postbuckling aerostructures, AIAA J. 43 (2008) 681–689, http://dx.doi.org/10.2514/1.7914.

[42] Re-steel, invar 36 for composite tooling (commercial catalog), 2021, pp. 2–3, https://re-steel.com/invar-plate/invar-36/.

[43] J. Singer, J. Arbocz, T. Weller, Buckling Experiments: Experimental Methods in Buckling of Thin-Walled Structures, John Wiley & Sons, Inc., Hoboken, NJ, USA, 2002, http://dx.doi.org/10.1002/9780470172995.